

Manuscript Details

| | |
|-------------------|--|
| Manuscript number | COST_2018_788 |
| Title | On Manufacturing Constraints for Tow-steered Composite Design Optimization |

Abstract

Automatic fiber placement machines have made it viable to manufacture composites where fiber angles vary continuously—tow-steered composites. The additional freedom provided by tow-steered composites have the potential to increase the structural performance, but also makes the design process more challenging. Numerical optimization can address this challenge, but it is critical to enforce constraints such that the resulting optimal tow-steered designs can be produced using current automatic fiber placement machines. In this work, we consider two manufacturing constraints: fiber path curvature and gaps/overlaps. To develop these constraints, we consider a general tow-steered layer pattern as a 2D unit vector field, where the field streamlines represent the tow paths laid down by the automated fiber placing machine. This mathematical formulation provides a relationship between fiber path curvature, gap/overlap propagation rate, vector curl, and divergence. These relationships also lead to a constraint on the minimum cut/add length of a tow for a given tow-steered pattern. We demonstrate the developed constraint formulations on two analytical examples, as well as on a structural optimization. We also explore the relationship between curl and divergence of rotated tow patterns. Finally, we use these relationships to motivate a family of gap/overlap-free and curvature-free tow-steered patterns.

Submission Files Included in this PDF

File Name [File Type]

manufacturing-constraints-tow.pdf [Manuscript File]

To view all the submission files, including those not included in the PDF, click on the manuscript title on your EVISE Homepage, then click 'Download zip file'.

On Manufacturing Constraints for Tow-steered Composite Design Optimization

Timothy R. Brooks*, Joaquim R. R. A. Martins

*University of Michigan, Department of Aerospace Engineering, Ann Arbor, Michigan,
United States*

Abstract

Automatic fiber placement machines have made it viable to manufacture composites where fiber angles vary continuously—tow-steered composites. The additional freedom provided by tow-steered composites have the potential to increase the structural performance, but also makes the design process more challenging. Numerical optimization can address this challenge, but it is critical to enforce constraints such that the resulting optimal tow-steered designs can be produced using current automatic fiber placement machines. In this work, we consider two manufacturing constraints: fiber path curvature and gaps/overlaps. To develop these constraints, we consider a general tow-steered layer pattern as a 2D unit vector field, where the field streamlines represent the tow paths laid down by the automated fiber placing machine. This mathematical formulation provides a relationship between fiber path curvature, gap/overlap propagation rate, vector curl, and divergence. These relationships also lead to a constraint on the minimum cut/add length of

*Corresponding author at: University of Michigan, Department of Aerospace Engineering, Ann Arbor, Michigan, United States.

Email address: timryanb@umich.edu (Timothy R. Brooks)

a tow for a given tow-steered pattern. We demonstrate the developed constraint formulations on two analytical examples, as well as on a structural optimization. We also explore the relationship between curl and divergence of rotated tow patterns. This leads to the conclusion that for layups featuring such patterns a stricter constraint bound must be used to satisfy the manufacturing constraint for each pattern, as opposed to if each pattern was allowed to vary independently. Finally, we use these relationships to motivate a family of gap/overlap-free and curvature-free tow-steered patterns.

Keywords: Variable angle tow, Optimization, Tow steering, Automated fiber placement, Manufacturing constraints

¹ 1. Introduction

² A conventional composite laminate is typically composed of a number
³ of layers featuring stiff fibers embedded in a softer matrix. The fibers in
⁴ each layer are usually fixed to the same orientation, where the orientation
⁵ alternates only from layer to layer (e.g., $0^\circ, \pm 45^\circ, 90^\circ$). While these restric-
⁶ tions ease the process of manufacturing, they are not necessarily structurally
⁷ ideal for distributing loads. With the advent of automatic fiber placement
⁸ (AFP) machines, we are no longer restricted to fixed fiber orientation within
⁹ a layer. AFP machines are capable of laying down fibers in strips of prepreg
¹⁰ tape along general curvilinear tow paths in each layer of the laminate. This
¹¹ process is known as tow-steering and provides the ability to locally specify
¹² the fiber direction for each layer of the laminate. Figure 1 shows a typical
¹³ conventional and tow-steered composite laminate.

¹⁴ The ability of variable angle tow (VAT) or tow-steered laminates to re-

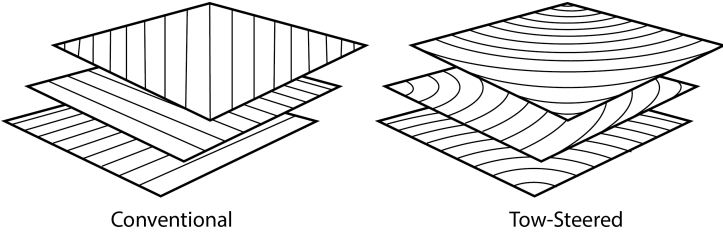
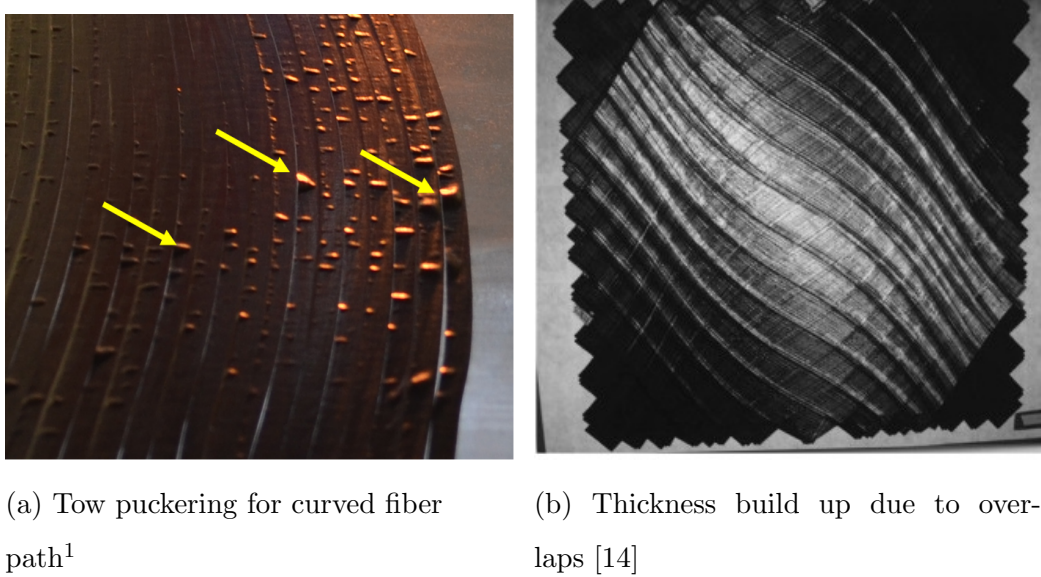


Figure 1: Example comparison of conventional (left) and tow-steered (right) layups.

15 distribute load paths in plate structures is an active field of research, and
 16 various authors have studied the benefit of tow-steering through the opti-
 17 mization of the continuous tow-paths for various plate structures. This in-
 18 cludes studies showing that tow-steered panels can be tailored for maximum
 19 strength [1, 2, 3] and for optimal buckling performance [4, 5, 6, 7, 8, 9, 10].
 20 The ability of tow-steered structures to mitigate stress concentrations around
 21 structural discontinuities, such as holes, has been another topic of inter-
 22 est [6, 3, 11, 10, 12]. All of these accomplishments are made possible by the
 23 ability of tow-steered laminates to more effectively redistribute loads.

24 While the improvements cited in the above work are impressive, there
 25 is a need for considering manufacturing constraints in the design of VAT
 26 composites [13]. Two of the most common manufacturing constraints related
 27 to AFP layup are the minimum tow path turning radius, and the presence
 28 of gaps and overlaps. The minimum turning radius of the tow path, R_{\min} ,
 29 is typically defined by the manufacturer to prevent the prepreg tow from
 30 twisting over itself or puckering out of plane as the tow is laid down by the
 31 head of the AFP machine. An example of tow puckering can be seen in
 32 Figure 2a. More aggressive values of minimum turning radii can be achieved
 33 by laying down paths with narrower prepreg tow, but for the same layup



(a) Tow puckering for curved fiber path¹

(b) Thickness build up due to overlaps [14]

Figure 2: Example of tow-steering defects due to AFP layup process

34 area this leads to an increase in manufacturing time and cost.
 35 The gaps and overlaps of the prepreg tow appear due to the geometric
 36 limitations of covering an area with fixed width tape and varying tow angle.
 37 As the tow is laid down, there are regions in the layup that are either void,
 38 or where two portions of adjacent tows overlap. Depending on the design
 39 application, gaps and overlaps may be considered to be defects. If not ac-
 40 counted for in the numerical model of the structure, these regions can lead
 41 to deviations in the predicted and actual stiffness and mass properties of
 42 the manufactured design. Additionally, these regions can potentially lead
 43 to unwanted thickness variations if they are allowed to build up during the
 44 layup process (see Figure 2b). Furthermore, tow-steered layups featuring
 45 excessively large gaps and overlaps may be difficult to manufacture, leading
 46 to further increases in manufacturing cost and time.

47 Many of the previously mentioned studies have included considerations
 48 for manufacturing constraints. The most common constraint considered is
 49 the minimum tow path turning radius [15, 7, 9]. The effect of gaps and
 50 overlaps on the local thickness of a tow-steered laminate was considered by
 51 Blom et al. [16]. The authors accomplished this by defining the tow paths as
 52 streamlines of a 2D stream function, analogous to that seen in aerodynamic
 53 theory. In their work, an optimization was performed with the objective
 54 being to minimize the thickness buildup due to prepreg tow overlap. In
 55 this work, we take an alternative approach, where an arbitrary tow-steered
 56 pattern is defined as a 2D unit vector field. This definition allows for the
 57 manufacturing constraints of fiber path curvature and gaps/overlaps to be
 58 related to the curl and divergence of the vector field, respectively. Figure 3
 59 provides a preview of how these two quantities can be used to identify regions
 60 of manufacturing difficulty in a layup.

61 **2. Curl-Curvature Divergence-Gap/Overlap Relationship**

62 Consider a 2D unit vector field, \vec{v} , defined by a tow-angle distribution,
 63 $\theta(x, y)$, as shown in Figure 4, such that:

$$64 \quad \vec{v}(\theta) = \cos(\theta)\hat{\mathbf{i}} + \sin(\theta)\hat{\mathbf{j}} \quad (1)$$

65 For the sake of conciseness, θ 's explicit dependence on x and y is omitted.
 66 The streamlines of the vector field \vec{v} represent the ideal tow paths of the
 67 tow-steered laminate ply. The circulation of the fiber paths per unit area
 68 can be measured by taking the curl of the vector field. Performing the curl

¹Courtesy of Benjamin Smith from the Aurora Flight Sciences company

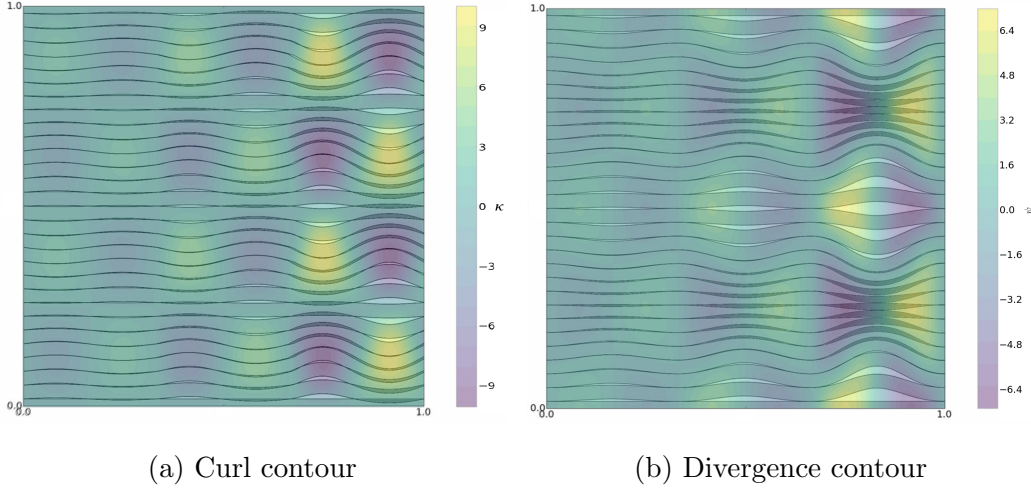


Figure 3: The curl, κ , and divergence, ψ , contours can be used to identify regions of manufacturing difficulty.

⁶⁹ operation on the vector field and taking the only non-zero vector component
⁷⁰ gives:

$$\kappa(x, y) = (\nabla \times \vec{v}(\theta)) \cdot \hat{\mathbf{k}} = \left(\nabla \times \left(\cos(\theta) \hat{\mathbf{i}} + \sin(\theta) \hat{\mathbf{j}} \right) \right) \cdot \hat{\mathbf{k}} = \frac{\partial \theta}{\partial x} \cos(\theta) + \frac{\partial \theta}{\partial y} \sin(\theta) = \nabla \theta \cdot \vec{v}(\theta) \quad (2)$$

⁷² This states that the curl of the vector field is the directional derivative of the angle, θ , in the tangential direction, \vec{v} , which is the definition of the curvature for a parametric curve.

While the relationship between curl and curvature is clear from the derivation above, the same is not the case for the relationship between divergence and gaps/overlaps. This relationship can be motivated by drawing an arbitrarily small control volume, Ω , and taking the flux per unit area, ψ , of the fiber paths passing through its boundary, C , as shown in Figure 5. The flux

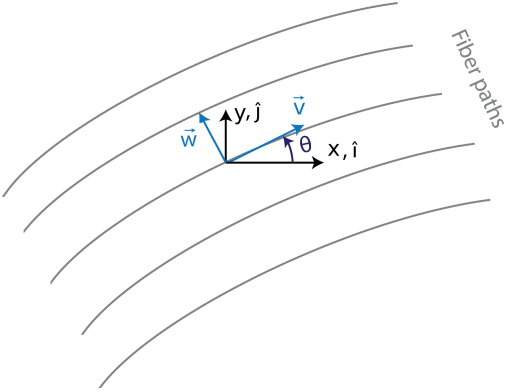


Figure 4: Tow path vector definitions.

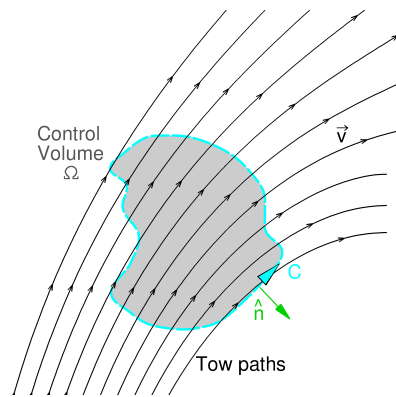


Figure 5: The divergence quantifies the flux of tow paths through an arbitrary control volume.

80 of fiber paths per unit area is then given by the limit:

81

$$\psi = \lim_{|\Omega| \rightarrow 0} \frac{1}{|\Omega|} \oint_C \vec{v} \cdot \hat{\mathbf{n}} \, ds,$$

82 where $|\Omega|$ is the area of Ω . From the above definition the units for ψ are
83 clearly $[\text{Length}]^{-1}$. Through the use of Gauss's theorem, this quantity can
84 be directly related to the vector field divergence:

85

$$\psi = \nabla \cdot \vec{v} \quad (3)$$

86 Substituting Equation (1) into the above, we get:

87

$$\psi(x, y) = \nabla \cdot \vec{v}(\theta) = \nabla \cdot (\cos(\theta)\hat{\mathbf{i}} + \sin(\theta)\hat{\mathbf{j}}) = \frac{\partial \theta}{\partial x}(-\sin(\theta)) + \frac{\partial \theta}{\partial y}(\cos(\theta)) = \nabla \theta \cdot \vec{w}(\theta), \quad (4)$$

88 where \vec{w} is the in-plane unit normal vector to the fiber path tangent vector
89 \vec{v} . Thus, analogously to the curvature, the divergence is the directional
90 derivative of the angle in the transverse direction.

91 At this point, we still have yet to make a connection between ψ and the
92 gap/overlap formation of the pattern. This relationship can be intuitively
93 shown through the following qualitative argument. If $\psi > 0$ in a region of the
94 pattern, then the density of fiber paths entering the control volume is larger
95 than that of the exiting fiber paths, indicating that a gap is likely to form.
96 Likewise, if $\psi < 0$, the fiber paths exiting the volume have greater density
97 than those entering, indicating that an overlap is likely to form. Finally, if
98 $\psi = 0$, the density of fiber paths entering and exiting the volume are equal
99 and no gap/overlap growth are expected. This means that, according to
100 Equation (4), the local tow paths should be as close to parallel as possible
101 to reduce the likelihood of gaps and overlaps in the pattern.

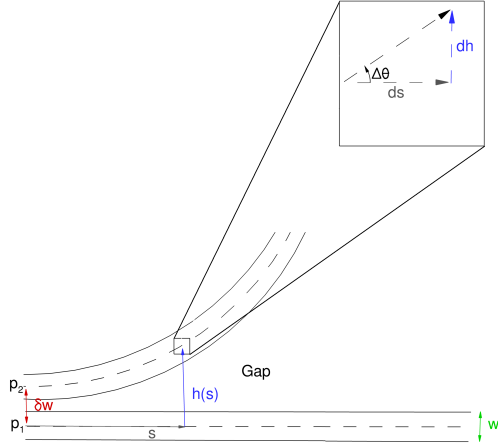


Figure 6: Gap propagation between two adjacent tow paths.

Now that we developed a qualitative relationship, we can proceed to derive a more quantitative relationship. First, consider two adjacent fiber paths, p_1 and p_2 , whose streamlines define the centerlines for two prepreg tow strips of width w , as shown in Figure 6. We assume that the centerlines of these tow paths are initially separated by a distance δw , where δ is the shift distance of the adjacent tow strip in percent tow width. If $\delta < 1$, the initial offset between the adjacent tow paths is smaller than the tow width, leading to an initial overlap. Likewise, if $\delta > 1$, there is a gap at the initial seeding points for the tows. Finally, if $\delta = 1$, the edges of the tow are coincident and there is no gap or overlap initially.

To find how the gap or overlap between these two tow paths propagate, we first need to find the separation between the two paths as a function of arc-distance traveled, $h(s)$. This separation distance is measured perpendicularly

₁₁₅ to path 1, p_1 . By drawing an infinitesimal triangle along p_2 , we derive:

$$\text{116} \quad dh = \tan(\Delta\theta(s)) ds \quad (5)$$

₁₁₇ As long as the angle between the two tow path directions is small, we can
₁₁₈ use the approximation:

$$\text{119} \quad \tan(\Delta\theta(s)) \approx \Delta\theta(s) \quad (6)$$

₁₂₀ Substituting this into Equation (5) yields:

$$\text{121} \quad dh = \Delta\theta(s) ds \quad (7)$$

₁₂₂ Next, by realizing that the angle between the two tow paths can be approximated by the directional derivative of θ in the transverse direction of p_1 , and
₁₂₃ recognizing the definition of divergence from Equation (4) gives:

$$\text{125} \quad \Delta\theta(s) \approx \nabla\theta \cdot h \vec{w}(s) = h \psi(s) \quad (8)$$

₁₂₆ Substituting this into Equation (7) and moving both h terms to the same
₁₂₇ side yields:

$$\text{128} \quad \frac{dh}{h} = \psi(s) ds$$

₁₂₉ Next, integrating both sides and remembering that by definition $h(0) = \delta w$,
₁₃₀ we get:

$$\text{131} \quad \int_{\delta w}^{h(s)} \frac{dh}{h} = \int_0^s \psi(s') ds'$$

₁₃₂ Evaluating the left integral

$$\text{133} \quad \ln\left(\frac{h(s)}{\delta w}\right) = \int_0^s \psi(s') ds'$$

₁₃₄ Next, moving everything but $h(s)$ to the right hand side reveals the desired
₁₃₅ relationship:

$$\text{136} \quad h(s) = \delta w \exp\left(\int_0^s \psi(s') ds'\right)$$

¹³⁷ Subtracting the tow width gives the distance between the edges of either tow
¹³⁸ or the height of the gap/overlap between them:

$$\text{¹³⁹ } h_{g/o}(s) = w \left(\delta \exp \left(\int_0^s \psi(s') ds' \right) - 1 \right) \quad (9)$$

¹⁴⁰ A positive value of $h_{g/o}$ indicates a gap, while a negative values indicates an
¹⁴¹ overlap. Finally, dividing by the tow width yields:

$$\text{¹⁴² } \frac{h_{g/o}}{w}(s) = \delta \exp \left(\int_0^s \psi(s') ds' \right) - 1 \quad (10)$$

¹⁴³ which is the gap/overlap nondimensionalized with respect to tow width.

¹⁴⁴ Comparing this quantitative relationship between the gap/overlap size
¹⁴⁵ and divergence to the qualitative argument made earlier reveals that the two
¹⁴⁶ are in good agreement. If $\psi(s) < 0$, then $h_{g/o}/w$ asymptotically decays to a
¹⁴⁷ value of -1 , indicating 100% overlap. This result should makes sense, since
¹⁴⁸ overlaps greater than this should not be possible. Conversely, if $\psi(s) > 0$,
¹⁴⁹ then $h_{g/o}/w$ grows positively, indicating a growing gap. Though this quan-
¹⁵⁰ tity is unbounded from above in theory, this relationship breaks down for
¹⁵¹ large gap sizes. If $\psi(s) = 0$, then $h_{g/o}/w$ remains constant, indicating no
¹⁵² gap/overlap growth.

¹⁵³ Equation (10) leads to the conclusion that the percentage gap/overlap in
¹⁵⁴ a region of the pattern is independent of the tow width used to lay up the
¹⁵⁵ pattern. This means that as the width of tow is decreased, the total area of
¹⁵⁶ gaps and overlaps in the layup remains constant. This is because according
¹⁵⁷ to Equation (9), the size of the gaps and overlaps in the layup scale linearly
¹⁵⁸ with tow size (i.e., $\mathcal{O}(w)$), while the number of gaps and overlaps scales with
¹⁵⁹ the inverse of tow width (i.e., $\mathcal{O}(1/w)$), since more tow paths mean more
¹⁶⁰ adjacent regions for gaps and overlaps to occur. This means the total area of

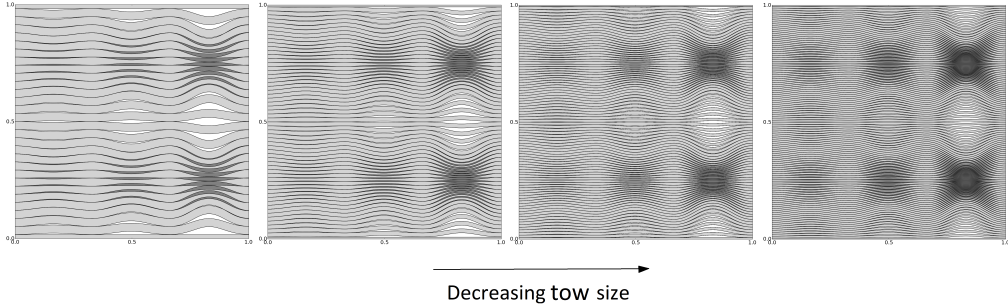


Figure 7: Example layup shows that gaps and overlaps do not improve as tow width is decreased.

161 gap or overlap in the pattern must scale with $\mathcal{O}(w/w) = \mathcal{O}(1)$, or in other
162 words remain constant. This effect can be seen clearly in Figure 7.

163 To verify the accuracy of Equation (10), one of the patterns from Figure 7 is seeded at two tow locations. The exact percentage of gap or overlap
164 adjacent to the strip is then compared to the approximate value predicted
165 by Equation (10). The results for both tow paths are shown in Figure 8.
166 From these plots, we can see that the approximate values predicted by Equa-
167 tion (10) are in good agreement with the actual size of gaps measured in the
168 layup. The gap/overlap size measured by Equation (10) is only on one side
169 of the tow. In the case of an overlap, this value should be doubled to get the
170 total overlap area for both sides of the strip, by symmetry.

172 Next, we wish to use Equation (10) to derive an alternate, and perhaps
173 more physically meaningful, interpretation of the divergence, ψ . This can
174 be revealed by first differentiating Equation (10) with respect to s , as shown
175 below:

$$\frac{d(h_{g/o}/w)}{ds}(s) = \psi(s)\delta \exp\left(\int_0^s \psi(s') ds'\right) \quad (11)$$

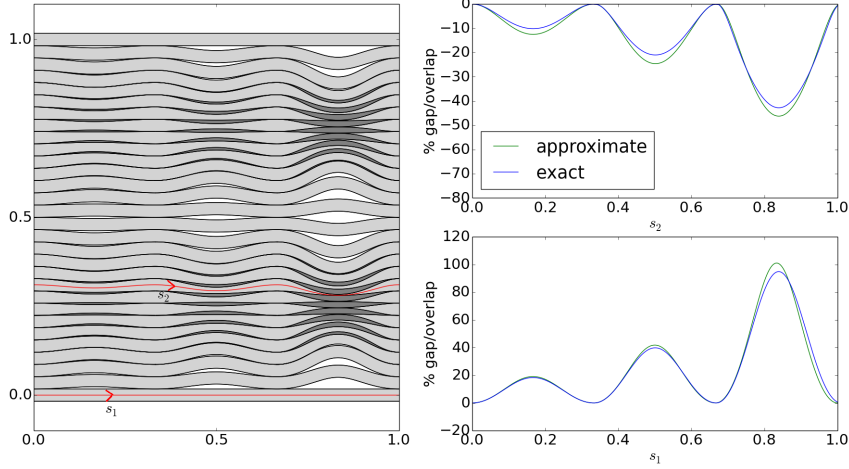


Figure 8: The predicted gap/overlap propagation agrees well with actual measured amount for example layup.

¹⁷⁷ Finally, recognizing that in regions where the gaps or overlap is small:

$$\delta \exp \left(\int_0^s \psi(s') ds' \right) \approx 1 \quad (12)$$

¹⁷⁹ Substituting this into Equation (11) yields:

$$\frac{d(h_{g/o}/w)}{ds}(s) \approx \psi(s), \quad (13)$$

¹⁸¹ which leads to an alternate, but equivalent, interpretation of the divergence.

¹⁸² The divergence, ψ , in a region of a pattern can be approximately defined as
¹⁸³ the rate of growth of small gaps/overlaps as a fraction of tow width per unit
¹⁸⁴ length of tow laid. This means that, for example, laying down tow in a region
¹⁸⁵ featuring a divergence value of 0.2 m^{-1} corresponds to a gap growth rate of
¹⁸⁶ 20% per meter. This definition provides a more intuitive way of specifying
¹⁸⁷ the divergence as a manufacturing constraint, since it relates to gap/overlap
¹⁸⁸ growth.

189 **3. Analytical Examples**

190 In the previous section, we derived mathematical relationships for the
191 tow-path curvature and gap/overlap propagation for a general tow pattern.
192 To give an example of how these equations can be applied, we consider two
193 simple tow patterns in this section. The patterns are chosen to be simple
194 so that analytical expressions can be derived for their relevant quantities,
195 and so that the results can provide an intuitive feel for the mathematical
196 relationships.

197 *3.1. Radially Diverging Pattern*

198 The first pattern we consider is a tow pattern whose paths emanate radi-
199 ally outward from its center, as shown in Figure 10. It is convenient to write
200 this vector field in polar coordinates:

201 $\vec{v} = \hat{\mathbf{r}}$

202 The curl and divergence of a vector field in polar coordinates, $\vec{v} = v_r \hat{\mathbf{r}} + v_\theta \hat{\theta}$,
203 is:

204 $\kappa(\theta, r) = (\nabla \times \vec{v}) \cdot \hat{\mathbf{k}} = \frac{1}{r} \left(\frac{\partial r v_\theta}{\partial r} + \frac{\partial v_r}{\partial \theta} \right), \quad \psi(\theta, r) = \nabla \cdot \vec{v} = \frac{1}{r} \left(\frac{\partial(r v_r)}{\partial r} + \frac{\partial v_\theta}{\partial \theta} \right)$

205 Substituting in for the vectors components yields the curvature and diver-
206 gence:

207 $\kappa(\theta, r) = 0, \quad \psi(\theta, r) = \frac{1}{r}$

208 It should come as no surprise that the curvature is zero for this pattern, since
209 all of the tow paths are straight lines. The divergence features a singularity
210 at the center and decays with the inverse distance from the origin. The

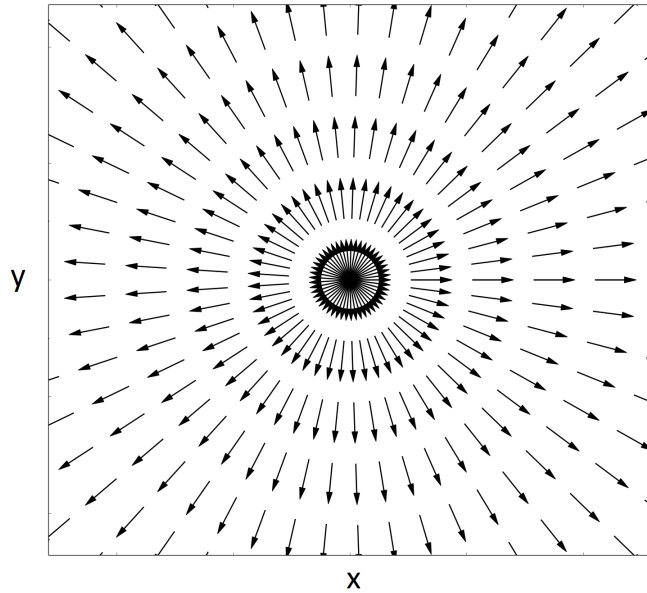


Figure 9: Tow path vector field, \vec{v} , for radially diverging tow pattern.

211 divergence decays to zero far away from the center of the pattern, since all
212 tow paths become more locally parallel further away from the center.

213 To derive the gap propagation, $h_{g/o}/w(s)$, suppose we begin laying the
214 prepreg tow down radially outward starting at a distance, R , from the center
215 (see Figure 10). The edges of the tows are assumed to be coincident at their
216 initial seed location, $s = 0$, implying that $\delta = 1$. The divergence as a function
217 of distance traveled along one of the tow paths, $\psi(s)$, is given by:

$$\psi(s) = \frac{1}{s + R}$$

219 Substituting the divergence, $\psi(s)$, into Equation (10) yields:

$$\frac{h_{g/o}}{w}(s) = \exp\left(\int_0^s \frac{1}{s' + R} ds'\right) - 1$$

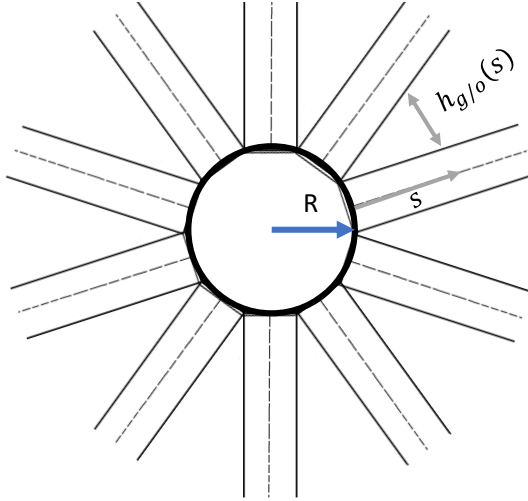


Figure 10: Gap definition for radial diverging pattern.

²²¹ Evaluating the integral we get:

$$\frac{h_{g/o}}{w}(s) = \left| \frac{s}{R} + 1 \right| - 1 \quad (14)$$

²²⁴ As long as $s \geq -R$, this can be further simplified to:

$$\frac{h_{g/o}}{w}(s) = \frac{s}{R} \quad (15)$$

²²⁶ This states that the adjacent gaps between tow strips grow linearly as the
²²⁷ tow is laid down. By evaluating Equation (15) at $s = -R$, we can show
²²⁸ that if the tow path were to be continued backward, toward the center, there
²²⁹ would exist a 100% overlap at the pattern's singularity. This conclusion can
²³⁰ be quickly verified by analyzing Figure 10.

²³¹ *3.2. Patterns with Linear Angle Variation*

²³² A common tow pattern parametrization scheme developed for tow-steered
²³³ composites is the linear angle variation scheme [2, 17, 8, 9, 12, 18]. This

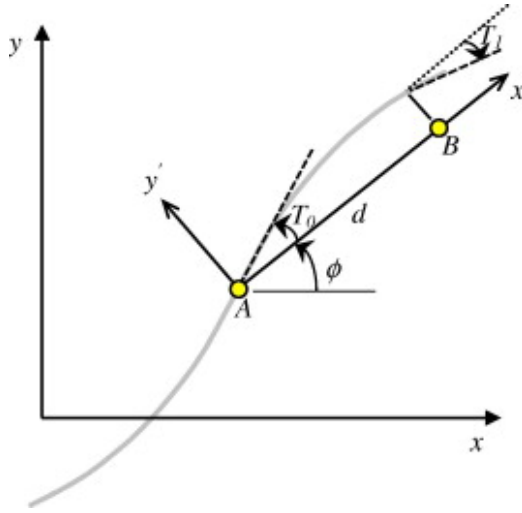


Figure 11: Linear-varying tow angle proposed by Gurdal et al. [17].

234 scheme was originally proposed by Olmedo and Gurdal [18]. In their work,
 235 they define the tow angle as varying piece-wise linearly along the x' -axis.
 236 The tow pattern is then parametrized by the fiber angle at the origin of the
 237 reference path, T_0 , and the angle at the edges of the laminate, T_1 , where
 238 $x' = [0, 2d]$. Thus the angle variation is:

$$\theta(x') = \begin{cases} \phi + \frac{T_0 - T_1}{d}x' + T_1, & \text{for } 0 \leq x' < d \\ \phi + \frac{T_1 - T_0}{d}(x' - d) + T_0, & \text{for } d \leq x' \leq 2d \end{cases} \quad (16)$$

240 They also introduced a compact notation for the pattern as $\phi \langle T_0, T_1 \rangle$. Fig-
 241 ure 11 shows an example of the tow path resulting from the linear angle
 242 distribution described above. For simplicity, we assume that $\phi = 0$, and thus
 243 $x = x'$. However, the following derivation can be generalized for $\phi \neq 0$.

244 The curvature and divergence of the tow path can be found by applying

²⁴⁵ Equations (2) and (4), respectively, to Equation (16).

$$\kappa(x) = \frac{d\theta}{dx}(x) \cos(\theta(x)) = \begin{cases} \frac{T_0-T_1}{d} \cos(\theta(x)), & \text{for } 0 \leq x < d \\ -\frac{T_0-T_1}{d} \cos(\theta(x)), & \text{for } d \leq x \leq 2d \end{cases}$$

$$\psi(x) = -\frac{d\theta}{dx}(x) \sin(\theta(x)) = \begin{cases} -\frac{T_0-T_1}{d} \sin(\theta(x)), & \text{for } 0 \leq x < d \\ \frac{T_0-T_1}{d} \sin(\theta(x)), & \text{for } d \leq x \leq 2d \end{cases}$$

²⁴⁹ Next, we derive the gap propagation, $h_{g/o}/w$, using Equation (10). We
²⁵⁰ assume that the AFP tow paths begin on the left side, $x = 0$, of the pat-
²⁵¹ tern. Performing an integration variable transformation from s' to θ in Equa-
²⁵² tion (10) gives:

$$\frac{h_{g/o}}{w}(x) = \delta \exp \left(\int_{\theta(0)}^{\theta(x)} \frac{\psi(\theta)}{\frac{\partial \theta}{\partial s}(\theta)} d\theta \right) - 1$$

²⁵⁴ Recognizing the definition of curvature (i.e., $\partial \theta / \partial s = \kappa$) and substituting in
²⁵⁵ the relevant expressions yields:

$$\frac{h_{g/o}}{w}(x) = \delta \exp \left(- \int_{T_1}^{\theta(x)} \frac{\sin(\theta)}{\cos(\theta)} d\theta \right) - 1 = \delta \exp \left(- \int_{T_1}^{\theta(x)} \tan(\theta) d\theta \right) - 1$$

²⁵⁷ Finally, evaluating the integral and manipulating variables gives:

$$\begin{aligned} \frac{h_{g/o}}{w}(x) &= \delta \exp (\ln(|\sec(T_1)|) - \ln(|\sec(\theta(x))|)) - 1 \\ &= \delta \exp \left(\ln \left(\left| \frac{\sec(T_1)}{\sec(\theta(x))} \right| \right) \right) - 1 \\ &= \delta \left| \frac{\sec(T_1)}{\sec(\theta(x))} \right| - 1 \\ &= \delta \left| \frac{\cos(\theta(x))}{\cos(T_1)} \right| - 1 \end{aligned} \tag{17}$$

263 Equation (17) is significant in that it provides us an analytical expression for
 264 the gap/overlap size as function of location in the pattern. A typical method
 265 for deciding the shift distance for adjacent tow paths is to space the tow
 266 paths such that either no gaps occur between adjacent paths (only overlaps),
 267 overlap method, or no overlaps occur (only gaps), gap method [19]. Table 1
 268 gives the corresponding shift distance, δ , for the gap and overlap methods.

Table 1: Shift parameter for gap/overlap method

| Condition | Overlap method | Gap method |
|--------------------------------|---|---|
| $ \cos(T_1) \leq \cos(T_0) $ | $\delta = \left \frac{\cos(T_1)}{\cos(T_0)} \right $ | $\delta = 1$ |
| $ \cos(T_1) > \cos(T_0) $ | $\delta = 1$ | $\delta = \left \frac{\cos(T_1)}{\cos(T_0)} \right $ |

269 Next, the overlap propagation predicted in Equation (17) is compared
 270 with a laminate laid up by Tatting et al. [19]. In their work, the authors
 271 modeled and manufactured a 15 in. by 20 in. laminated plate, with a layup of
 272 $[\pm 45^\circ / \pm 45^\circ, 60^\circ]_2 / [\pm 30^\circ, 15^\circ]_2, [\pm 45^\circ, 60^\circ]_2]_s$ using the overlap method.
 273 The overlap pattern predicted by Equation (17) for the tow-steered layers of
 274 the laminate, $\pm 45^\circ, 60^\circ$ (dark gray) and $\pm 30^\circ, 15^\circ$ (light gray) are shown
 275 in Figure 12. From Figure 12, it can be seen that the overlap size predicted
 276 by Equation (17) and the tow spacing predicted by Table 1 are in good
 277 agreement with the overlap pattern found numerically by the authors.

278 4. Bound for Minimum Tow Cut and Addition Length

279 As mentioned previously, a number of studies have already considered
 280 the application of numerical design optimization to tow-steered laminates.

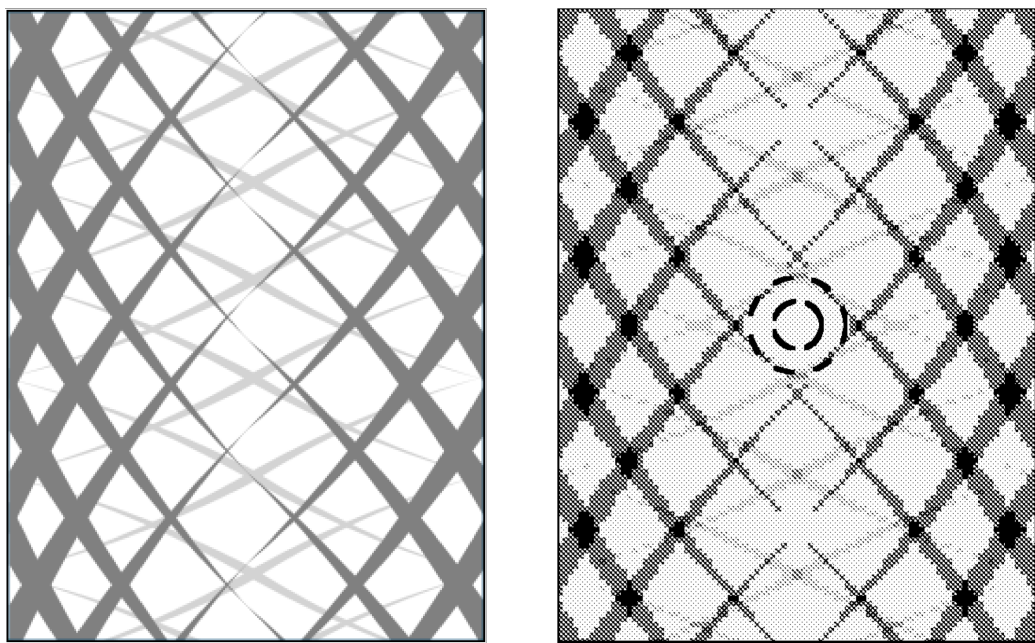


Figure 12: The prediction of the overlap size and spacing given by Equation (17) (left) match well with the that found by Tatting and Gurdal [19] (right).

281 In many of these works, the main manufacturing constraint considered is on
282 the minimum turning radius. This is usually enforced through a constraint
283 on the curvature magnitude, as given below:

284

$$-\frac{1}{R_{\min}} \leq \kappa \leq \frac{1}{R_{\min}}$$

285 However, there are a number of other manufacturing constraints relating to
286 tow gaps and overlaps that have yet to be considered as constraints in the
287 context of design optimization.

288 The first of these constraints is that of the tow minimum cut length,
289 L_{cut} . Tow paths are typically cut by the AFP machine in the layup process
290 to avoid regions of excessive overlap. This value, L_{cut} , refers to the smallest
291 length of tow that can be laid by the AFP machine before the tow can be cut.
292 This length is typically dictated by the distance between the spool storing
293 the prepreg tow and the cutting mechanism on the AFP machine. Figure 13
294 is an example of a tow pattern that fails to meet the minimum cut length
295 constraint. The second constraint is on the minimum tow addition length,
296 L_{add} . This defines the minimum amount of tow laid for two adjacent tow
297 paths before the machine may consider adding an additional tow in between
298 a gap of the current two. While the previous constraint was a limitation of
299 the AFP machine, this constraint is at the discretion of the designer. Smaller
300 values of L_{add} mean that additional tows need to be placed more frequently
301 in between gaps of adjacent tow paths, leading to higher manufacturing cost
302 and time.

303 Typically, AFP machines are programmed to add and drop tows based
304 on a gap and overlap percentage rule. For instance, if a gap between two
305 tow paths in a region exceeds a predefined gap percentage rule, $h_{g/o}/w \geq a_g$,

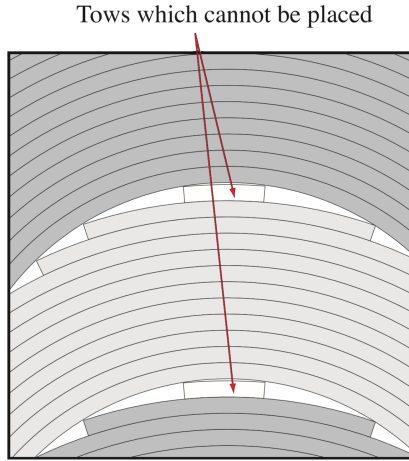


Figure 13: Example of minimum cut length restriction (Reproduced from Blom [20]).

306 the AFP machine starts a new tow centered between the gap of the previous
 307 two. Likewise, if the overlap between two tows exceeds the overlap percentage
 308 rule, $h_{g/o}/w \leq -a_o$, the machine is programmed to cut one of the tows. It
 309 is therefore reasonable to expect that both of the constraints defined above
 310 should depend on these values. A typical gap/overlap rule used by designers
 311 is a 50% gap/ 50% overlap rule, where $a_g = a_o = 0.5$.

312 Both L_{cut} and L_{add} can be evaluated explicitly for a given pattern using
 313 Equation (10). This requires a numerical integration and knowledge of the
 314 starting locations of AFP tow paths. In the context of a design optimization,
 315 however, this may be difficult to evaluate. Therefore, it would be beneficial
 316 to derive a conservative lower bound for these values independent of AFP
 317 seeding location.

318 This can be accomplished by considering the worst-case scenario for either
 319 case. As mentioned previously, a tow cut is only made by the machine when
 320 the overlap rule is about to be violated. This means that the worst-case to

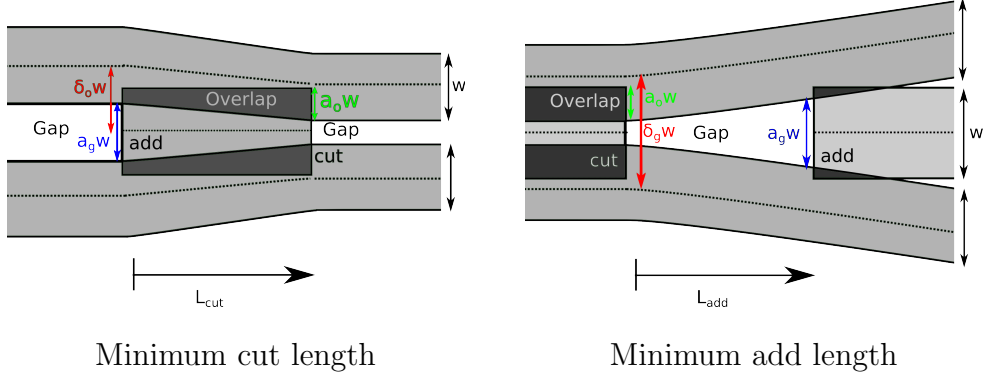


Figure 14: Example of worst-case scenario cut/add sizes.

analyze for cut length would be a case where the tow starts with some initial overlap value at its initial seeding location. This occurs at locations where a tow is added in a gap to prevent the gap rule from being violated. Likewise, worst-case for the add length occurs in regions where there is some initial amount of gap height at the beginning of this length. This typically occurs right after a tow is cut to satisfy the overlap rule. Figure 14 illustrates both of these cases.

Substituting the symbols from Figure 14 into Equation (10) yields:

$$-a_o = \delta_o \exp \left(\int_0^{L_{\text{cut}}} \psi(s') ds' \right) - 1, \quad a_g = \delta_g \exp \left(\int_0^{L_{\text{add}}} \psi(s') ds' \right) - 1 \quad (18)$$

By further analyzing Figure 14, we can derive the following relationships between the minimum cut/add length offsets (δ_o and δ_g), and the gap/overlap rules (a_g and a_o):

$$2\delta_o w = w + a_g w, \quad \delta_g w = w + (w - 2a_o w)$$

³³⁴ Solving for each offset parameter yields:

$$\delta_o = \frac{1 + a_g}{2}, \quad \delta_g = 2(1 - a_o) \quad (19)$$

³³⁶ Note that not all combinations of gap and overlap rules (a_g and a_o) are
³³⁷ permitted. We can see from Figure 14 when a tow is cut, a gap of size $\delta_g - 1$
³³⁸ is present immediately after the cut. If the resulting gap size already violates
³³⁹ the gap rule, then it is impossible to satisfy both the gap and overlap rule.

³⁴⁰ Thus, we require that:

$$\delta_g - 1 \leq a_g$$

³⁴² Substituting in for δ_o and rearranging terms leads to the following inequality:

$$a_g \geq 1 - 2a_o \quad (20)$$

³⁴⁴ Next, substituting Equation (19) into Equation (18) yields:

$$-a_o = \frac{1 + a_g}{2} \exp \left(\int_0^{L_{\text{cut}}} \psi(s') ds' \right) - 1, \quad a_g = 2(1 - a_o) \exp \left(\int_0^{L_{\text{add}}} \psi(s') ds' \right) - 1 \quad (21)$$

³⁴⁵ At this point, Equation (21) still depends on the AFP starting location of
³⁴⁶ the tow paths, implicitly, through the inclusion of the integration of the
³⁴⁷ divergence term, $\int_0^{L_{\text{cut}}} \psi(s') ds'$. From Figure 14, it is clear that $\psi(s) <$
³⁴⁸ 0 and $\psi(s) > 0$ for the worst-case scenario of the minimum cut and add
³⁴⁹ length, respectively. Thus, we can conservatively bound each integral in
³⁵⁰ Equation (21) by using the minimum and maximum divergence values in the
³⁵¹ pattern:

$$\psi_{\max} = \arg \max_{x,y} \psi(x,y), \quad \psi_{\min} = \arg \min_{x,y} \psi(x,y) \quad (22)$$

354 Equation (21) can then be further simplified by assuming the divergence
 355 remains constant in these regions. This leads to the relationship:

$$356 \quad -a_o = \frac{1+a_g}{2} \exp(\psi_{\min} L_{\text{cut}}) - 1, \quad a_g = 2(1-a_o) \exp(\psi_{\max} L_{\text{add}}) - 1$$

357 Finally, solving for the minimum and maximum divergence yields:

$$358 \quad \psi_{\min} = -\frac{\ln\left(\frac{1+a_g}{2(1-a_o)}\right)}{L_{\text{cut}}}, \quad \psi_{\max} = \frac{\ln\left(\frac{1+a_g}{2(1-a_o)}\right)}{L_{\text{add}}}$$

359 Using these values, a conservative bound can now be placed on the diver-
 360 gence everywhere in the tow pattern, as follows:

$$361 \quad -\frac{\ln\left(\frac{1+a_g}{2(1-a_o)}\right)}{L_{\text{cut}}} \leq \psi \leq \frac{\ln\left(\frac{1+a_g}{2(1-a_o)}\right)}{L_{\text{add}}} \quad (23)$$

362 This constraint ensures that the minimum cut and add lengths are respected
 363 regardless of choice of AFP seeding location. By further analyzing Equa-
 364 tion (23), it becomes clear that Equation (20) prevents either side of the
 365 bounds in Equation (23) from swapping signs. According to Equation (23),
 366 as $L_{\text{cut}}, L_{\text{add}} \rightarrow \infty$, the minimum cut/add length requirement becomes more
 367 strict and the divergence everywhere must drop to zero. Conversely, if
 368 $L_{\text{cut}}, L_{\text{add}} \rightarrow 0$, the minimum cut/add length requirement is relaxed, and
 369 the divergence becomes unbounded. If no overlaps are allowed (i.e. $a_o = 0$)
 370 and the gap rule is set to the smallest value allowed by Equation (20) (i.e.
 371 $a_g = 1$), the divergence is again forced everywhere to zero. If the overlap
 372 rule is relaxed and $a_o \rightarrow 1$, implying that tows never need to be cut, the
 373 divergence again becomes unbounded.

374 Equation (23) is a sufficient condition to guarantee that the minimum
 375 cut and add length restrictions are met, but it is not a necessary condition.

376 This means that if the divergence of a tow pattern exceeds these bounds, this
377 does not necessarily guarantee that the layup violates the minimum cut/add
378 length requirements. However, the only way to verify this for these patterns
379 is to check the cut/add lengths at each of the AFP seeding locations through
380 Equation (10).

381 **5. Stress Minimization Problem**

382 We now demonstrate the application of the constraints we just derived.
383 To this end, we perform a structural design optimization of a single-ply “L”-
384 shaped plate. The inner corner of the plate is filleted to ensure that the
385 stress remains bounded in this region. The plate is 5 mm thick, clamped
386 on one edge, and has a distributed shear force of 4 kN/m applied to one
387 of its free edges. The plate’s dimensions, loading, and boundary conditions
388 are shown in Figure 15. The material properties for the laminate are listed
389 in Table 2. The finite element analysis mesh used to model this problem
390 consists of approximately 7500 plate elements. Without having to solve the
391 finite-element problem, it is well known that a stress concentration occurs
392 at the corner of the plate. This stress concentration might be representative
393 of certain regions in a wingbox design where local stress concentrations are
394 expected to occur, such as the wing-fuselage intersection, Yehudi break of
395 the wing, or engine mounting location.

396 The structural solver used for this problem is the Toolkit for Analysis of
397 Composite Structures (TACS) [21]. TACS is a finite element method solver
398 that was developed to solve structures consisting of thin shell components,
399 which are typical in aerospace structures. The solver employs a parallel

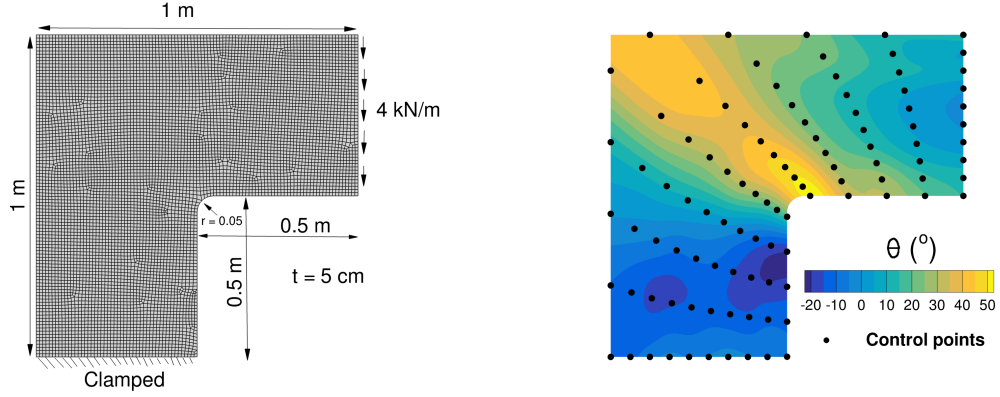


Figure 15: Problem loading/boundary conditions (left), design variables (right).

Table 2: Stress minimization problem material properties.

| Property | E_1 [GPa] | E_2 [GPa] | G_{12} [GPa] | G_{13} [GPa] | G_{23} [GPa] | ν_{12} | X_t [MPa] | X_c [MPa] | Y_t [MPa] | Y_c [MPa] | S_{12} [MPa] | ρ [kg/m ³] |
|----------|----------------|----------------|-------------------|-------------------|-------------------|------------|----------------|----------------|----------------|----------------|-------------------|--------------------------------|
| Value | 54.0 | 18.0 | 9.0 | 9.0 | 9.0 | 0.25 | 2410.0 | 1040.0 | 73.0 | 173.0 | 71.0 | 1550 |

400 direct factorization method, which allows it to efficiently solve the poorly-
 401 conditioned structural problems that are inherent in thin shell structures. In
 402 addition to computing the structural displacements, TACS computes other
 403 structural functions of interest, such as material failure and buckling loads.
 404 TACS also features an adjoint method for computing structural sensitivities
 405 with respect to large numbers of design variables efficiently [21, 22].
 406 These sensitivities enable the use efficient gradient-based optimization tech-
 407 niques. The optimizer used for this problem is the Sparse Nonlinear Opti-
 408 mizer (SNOPT) [23]. SNOPT is a quasi-Newton gradient-based optimizer
 409 designed for the optimization of large and sparse optimization problems.

410 The objective of the optimization problem is to minimize the maximum

⁴¹¹ Tsai–Wu stress in the plate, which is given by:

$$\sigma_{\text{TW}} = \sqrt{\frac{\sigma_{11}^2 + (X_c - X_t)\sigma_{11}}{X_t X_c} + \frac{\sigma_{22}^2 + (Y_c - Y_t)\sigma_{22}}{Y_t Y_c} + \left(\frac{\sigma_{66}}{S_{12}}\right)^2}, \quad (24)$$

⁴¹³ where σ_{11} , σ_{22} , and σ_{66} are the tangential, transverse, and shear stresses relative to the local fiber orientation; X_t/X_c and Y_t/Y_c are the tension and compression ply strengths parallel and transverse to fiber direction, respectively.
⁴¹⁴ Similarly, S_{12} is the ply shear strength in the fiber reference frame. The maximum stress is approximated by first evaluating the stress at each structural node, and then using a Kreisselmeier–Steinhauser (KS) aggregation [24, 25] over the domain of the plate. The design variables for the optimization problem are the fiber orientations, set through 100 B-spline control points, shown in Figure 15. The design problem includes two constraints. The first one is on the minimum turning radius, enforced by bounding the maximum and minimum fiber path curvature. As mentioned in Section 1, this is common manufacturing constraint that has been considered by number of previous authors. The second constraint is on the minimum cut and add lengths for the pattern, enforced by bounding the maximum and minimum fiber path divergence. This constraint, while analogous to the curvature is more novel in the context of design optimization of tow-steered layups. Similarly to the Tsai–Wu stress, the maximum and minimum curvature and divergence are approximated by computing the values at each node and aggregating them through another KS function. For this problem, the minimum turning radius, R_{\min} , is set to 0.1 m. We use a 50% gap and overlap rule for the minimum cut/add length constraint ($a_o = a_g = 0.5$). The optimization is performed four times with progressively stricter cut/add length constraints,

435 $L_{\text{cut}} = L_{\text{add}} = [0 \text{ m}, 0.025 \text{ m}, 0.1 \text{ m}, 0.4 \text{ m}]$. For the optimization case with
 436 $L_{\text{cut}} = L_{\text{add}} = 0 \text{ m}$, we remove the divergence constraint. While the presences
 437 of gaps and overlaps are constrained during the optimization, their effect on
 438 the local stiffness of the design is neglected. The optimization problem can
 439 be stated as:

$$\begin{aligned}
 & \text{minimize} && \text{KS}(\sigma_{\text{TW}}) \\
 & \text{with respect to} && \theta_{\text{cp}} \\
 & \text{such that} && -\frac{1}{R_{\min}} \leq \kappa \leq \frac{1}{R_{\min}} \\
 & && -\frac{\ln\left(\frac{1+a_g}{2(1-a_o)}\right)}{L_{\text{cut}}} \leq \psi \leq \frac{\ln\left(\frac{1+a_g}{2(1-a_o)}\right)}{L_{\text{add}}}
 \end{aligned}$$

440
 441 For this study, we start with an unsteered unidirectional design, as shown
 442 in Figure 16. From this results, we can see that as expected, a sharp stress
 443 concentration occurs at the interior corner of the plate. The results for all
 444 four optimization cases are shown in Figure 17. For all four tow-steered de-
 445 signs, the optimizer effectively redistributes the stress more uniformly over
 446 the domain of the plate, reducing the maximum stress by up to 68%. This
 447 significant reduction in stress concentration means that by tailoring the di-
 448 rectional stiffness properties of the composite, a less reinforced layup can be
 449 used in this region, which saves structural weight.

450 The design without the cut/add length constraints in Figure 17(a) per-
 451 forms the best in terms of objective value. While this design is the most
 452 effective in redistributing the structural loads, most of the fiber paths em-
 453 anate from a point on the right-most edge of the plate. In addition to this
 454 region, there are also several other locations in the pattern where fiber paths
 455 converge on each other. Plotting the fiber path divergence, ψ (Figure 17 (a))
 456 helps to highlight these regions. These regions are particularly problematic

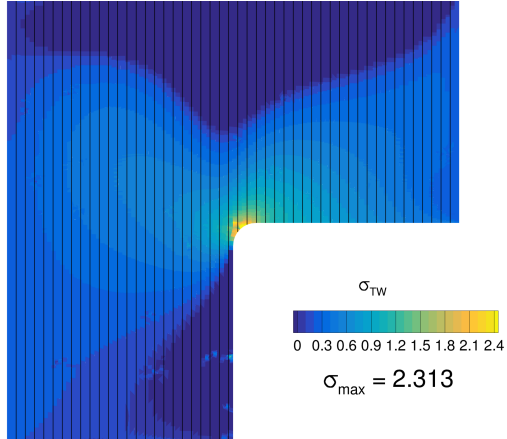


Figure 16: Unsteered baseline stress solution and tow paths.

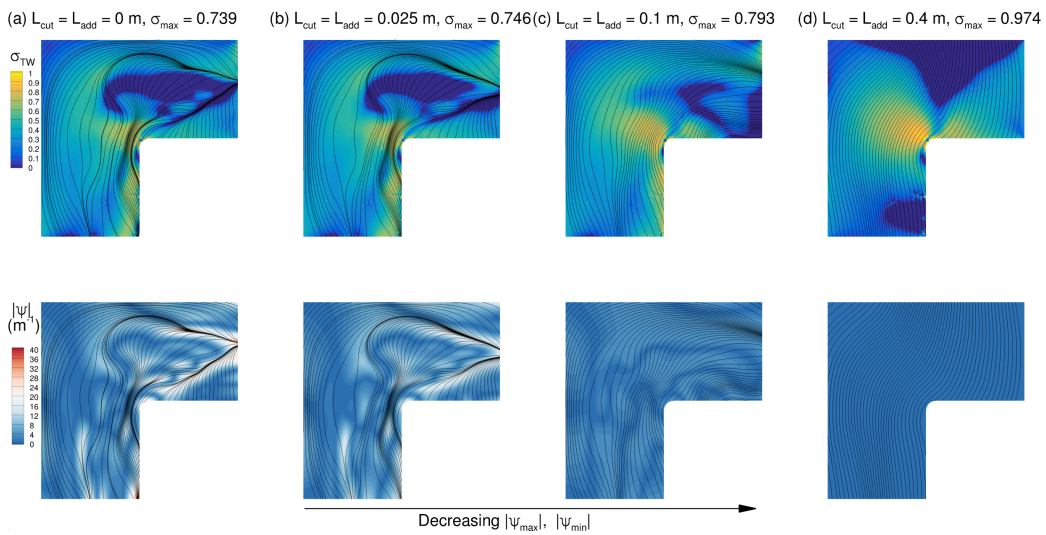


Figure 17: Optimization results showing Tsai–Wu stress (top) and fiber path divergence (bottom).

457 as they may lead to severe gaps and overlaps in the AFP layup process.
458 The results of the cut/add length-constrained optimizations are shown in
459 Figure 17 (b) - (d). As should be expected, the tow paths become more uni-
460 formly spaced as the constraint becomes more restrictive. The increasingly
461 restrictive constraint comes at a cost in objective performance. Nevertheless,
462 the most restrictive case (Figure 17 (d)) is still able to decrease the maximum
463 stress by 58% relative to the baseline design. This trend can be followed un-
464 til the desired minimum tow cut/add length in the design has been met, as
465 given by Equation (23).

466 6. Divergence-Curvature Relationship for Rotated Patterns

467 In theory, each layer of a tow-steered laminate can be parametrized with
468 its own unique pattern during the design process. In practice, however, as the
469 number of layers becomes very large, the number of design variables required
470 to parametrize the laminate may become too large for even gradient-based op-
471 timization to be practical. To simplify this, rather than parameterizing each
472 tow-steered layer independently, we can parametrize a main tow pattern and
473 define the remaining patterns in the layup as constant angular offsets rela-
474 tive to the main pattern. One design application where this parametrization
475 might be used is in the structural design of an aircraft wingbox [26, 27], where
476 the thickness of the laminate may be as high as $\mathcal{O}(100)$ layers in some parts
477 of the structure. We now derive a relationship between the divergence and
478 curvature of the offset patterns relative to the corresponding values of main
479 pattern.

480 We start by defining two tow path vector fields, \vec{v}_0 and \vec{v}_1 , parametrized

481 by angle distributions θ_0 and θ_1 , respectively. The two vector fields are
 482 related by the fact that \vec{v}_1 is offset from \vec{v}_0 by a constant angular offset, $\Delta\theta$,
 483 such that:

484
$$\theta_1 = \theta_0 + \Delta\theta$$

485 If we now take the curvature of the second vector field, we get:

486
$$\kappa_1(x, y) = \nabla\theta_1 \cdot \vec{v}_1(\theta_1) = \nabla\theta_1 \cdot (\cos(\theta_1)\hat{\mathbf{i}} + \sin(\theta_1)\hat{\mathbf{j}}) = \frac{\partial\theta_1}{\partial x} \cos(\theta_1) + \frac{\partial\theta_1}{\partial y} \sin(\theta_1) \quad (25)$$

487 Substituting in $\theta_1 = \theta_0 + \Delta\theta$ and using the fact that $\partial\theta_1/\partial x = \partial\theta_0/\partial x$ and
 488 $\partial\theta_1/\partial y = \partial\theta_0/\partial y$, and $\Delta\theta$ is a constant we obtain:

489
$$\kappa_1(x, y) = \frac{\partial\theta_0}{\partial x} \cos(\theta_0 + \Delta\theta) + \frac{\partial\theta_0}{\partial y} \sin(\theta_0 + \Delta\theta) \quad (26)$$

490 Finally, using the trigonometric identities $\cos(\theta_0 + \Delta\theta) = \cos(\theta_0)\cos(\Delta\theta) -$
 491 $\sin(\theta_0)\sin(\Delta\theta)$ and $\sin(\theta_0 + \Delta\theta) = \sin(\theta_0)\cos(\Delta\theta) + \cos(\theta_0)\sin(\Delta\theta)$, col-
 492 lecting terms, and recognizing the divergence and curvature terms derived
 493 previously, yields:

494
$$\begin{aligned} \kappa_1(x, y) &= \frac{\partial\theta_0}{\partial x}(\cos(\theta_0)\cos(\Delta\theta) - \sin(\theta_0)\sin(\Delta\theta)) + \frac{\partial\theta_0}{\partial y}(\sin(\theta_0)\cos(\Delta\theta) + \cos(\theta_0)\sin(\Delta\theta)) \\ 495 &= \left(\frac{\partial\theta_0}{\partial x} \cos(\theta_0) + \frac{\partial\theta_0}{\partial y} \sin(\theta_0) \right) \cos(\Delta\theta) + \left(\frac{\partial\theta_0}{\partial x}(-\sin(\theta_0)) + \frac{\partial\theta_0}{\partial y} \cos(\theta_0) \right) \sin(\Delta\theta) \\ 496 &= \kappa_0 \cos(\Delta\theta) + \psi_0 \sin(\Delta\theta) \end{aligned} \quad (27)$$

498 In a similar fashion, we can derive the following equation for the divergence:

499
$$\psi_1(x, y) = -\kappa_0 \sin(\Delta\theta) + \psi_0 \cos(\Delta\theta) \quad (28)$$

501 These relationships show that the divergence and curvature of two tow-
 502 steered patterns offset by a constant angle are inherently related. Note that

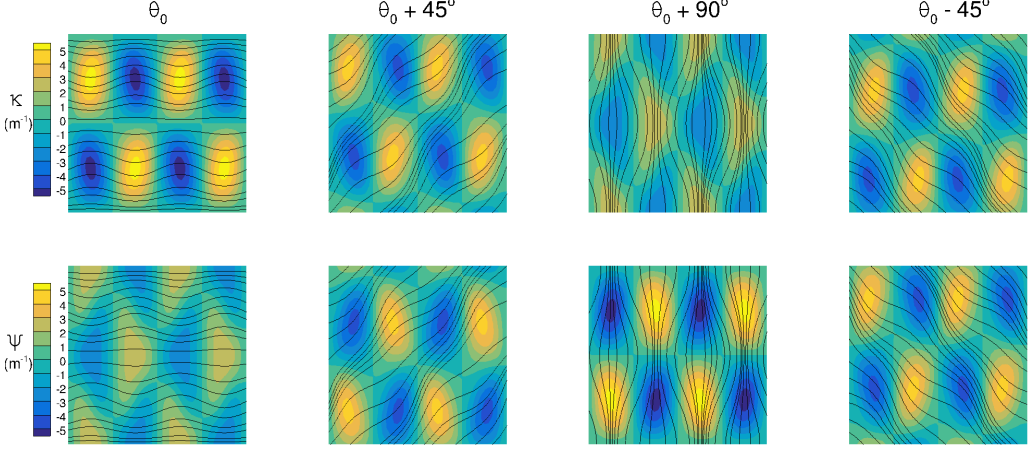


Figure 18: Example of the divergence-curvature relationship for offset patterns.

503 if the offset is exactly 90° , the divergence and curvature switch magnitudes
 504 between the two patterns. We can see this effect in Figure 18. This means
 505 that when considering multiple patterns offset by a constant angle, the more
 506 stringent of the two constraints (fiber divergence or fiber curvature) ends up
 507 being the active constraint for each ply.

508 7. Zero-Divergence and Zero-Curl Patterns

509 In Section 2 a relationship between the curl, divergence, fiber curvature,
 510 and gaps/overlaps for a general tow-steered pattern was derived. From this
 511 relationship, it is natural to wonder if there are tow-steered patterns with
 512 zero divergence, zero curl, or both everywhere in the layup. To answer this
 513 question, we can start by looking at a general pattern, \vec{v}_ψ , for which the
 514 divergence is zero.

$$515 \quad \nabla \cdot \vec{v}_\psi = 0 \quad (29)$$

516 From the principles of vector calculus, it is known that Equation (29) defines
 517 what is called a “incompressible” vector field. This means that vector field
 518 pattern can be defined as the curl of another vector field, as shown below:

$$519 \quad \vec{v}_\psi = \nabla \times \vec{\phi}(x, y) \quad (30)$$

520 Because \vec{v}_ψ is a 2D vector field, $\vec{\phi}$ must be orthogonal to the tow pattern
 521 field, \vec{v}_ψ , and therefore can be defined by a stream function, $\phi(x, y)$:

$$522 \quad \vec{\phi}(x, y) = \phi(x, y) \hat{\mathbf{k}} \quad (31)$$

523 Substituting Equation (31) into Equation (30) gives:

$$524 \quad \vec{v}_\psi = \frac{\partial \phi}{\partial y} \hat{\mathbf{i}} - \frac{\partial \phi}{\partial x} \hat{\mathbf{j}} \quad (32)$$

525 Finally, remembering that by definition \vec{v}_ψ should be a unit vector:

$$526 \quad \vec{v}_\psi \cdot \vec{v}_\psi = 1 \quad (33)$$

527 Substituting Equation (32) into Equation (33) yields:

$$528 \quad \frac{\partial \phi^2}{\partial x} + \frac{\partial \phi^2}{\partial y} = 1 \quad (34)$$

529 This is a very well-known nonlinear Partial Differential Equation (PDE), of-
 530 ten encountered in the fields of electro-magnetics and optics, known as the
 531 Eikonal equation. The solution, ϕ , to this equation is called a signed distance
 532 function. The function value at each point, $\phi(x, y)$, is defined as the distance
 533 from that point to a boundary curve, Ω , where the sign denotes which side
 534 of the boundary the point lies on. A common approach to obtaining these
 535 solutions is the fast marching method [28]. Since $\phi(x, y)$ is a stream function

536 of a 2D vector field, by definition, the stream lines of the tow patterns can
 537 be reproduced by plotting the iso-contours of ϕ . In this case, the curva-
 538 ture for these patterns can be computed by applying the curl, as defined in
 539 Equation (2), to Equation(32):

$$540 \quad \kappa_\psi = \left(\nabla \times \left(\frac{\partial \phi}{\partial y} \hat{\mathbf{i}} - \frac{\partial \phi}{\partial x} \hat{\mathbf{j}} \right) \right) \cdot \hat{\mathbf{k}} = - \left(\frac{\partial^2 \phi}{\partial x^2} + \frac{\partial^2 \phi}{\partial y^2} \right) = -\nabla^2 \phi \quad (35)$$

541 This equation provides an effective way of evaluating and constraining the
 542 curvature of any zero-divergence Eikonal solution.

543 This motivates an alternative approach to using B-spline interpolation to
 544 define the orientation field, $\theta(x, y)$, and subsequently the corresponding tow
 545 pattern, as described in Section 5. Instead, we can define the tow pattern
 546 as a level set function that is parametrized by the boundary, Ω . This is
 547 an approach that has seen growing interest in tow-steering design optimiza-
 548 tion [29, 30, 31].

549 By using Equation (27), a complementary family of zero-curl tow pat-
 550 terns, \vec{v}_κ , can be obtained by defining a corresponding orthogonal pattern to
 551 each zero-divergence solution. An alternative but equivalent definition for the
 552 zero-curl tow patterns is to define a number of seed locations on the bound-
 553 ary curve, Ω , and march out perpendicularly to the curve in all directions.
 554 A similar approach in the derivation of the zero-curl solution can be taken
 555 as the zero-divergence solution, leading back to the Eikonal equation (34),
 556 where ϕ now represents a scalar potential field, in this case $\vec{v}_\kappa = \nabla \phi$ and
 557 $\psi_\kappa = \nabla^2 \phi$.

558 Examples of zero-divergence and corresponding zero-curl patterns are
 559 shown in Figure 19. As one would expect from Equations (2) and (4), all of
 560 the paths for the divergence-free solutions are locally parallel, while the tow

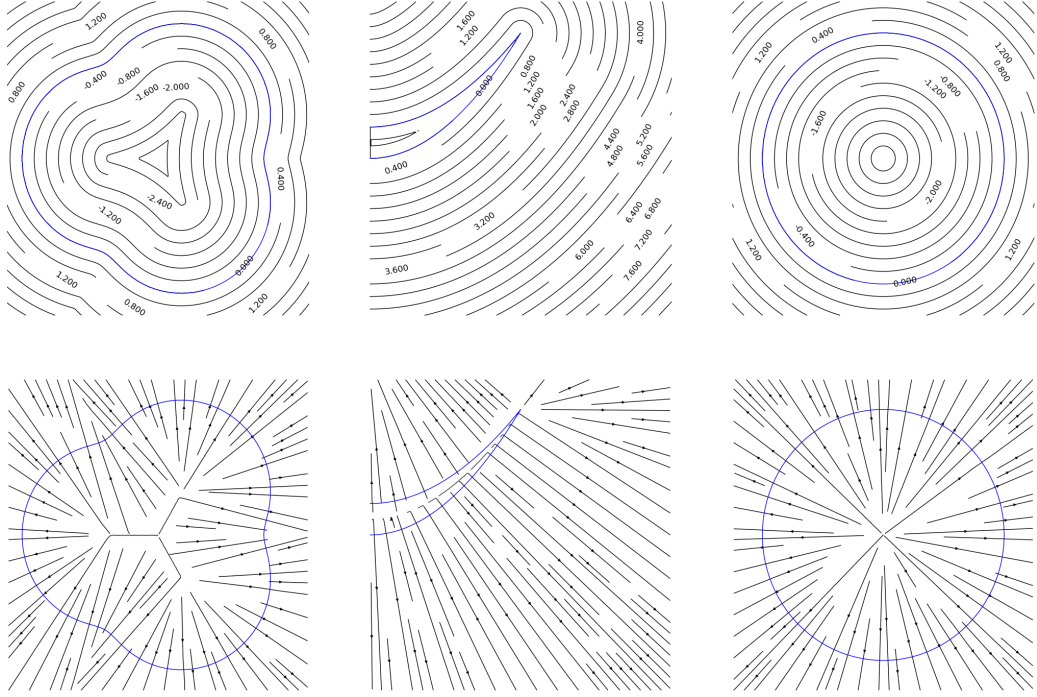


Figure 19: Zero-divergence (top) and corresponding zero-curl (bottom) Eikonal solutions, boundary curve, Ω (blue).

561 orientation remains constant along tow-paths for the curl-free solutions.

562 If Ω has no local curvature, that is if Ω is piece-wise linear, the resulting
 563 pattern will feature no curvature nor divergence. Figure 20 shows examples
 564 of patterns featuring both zero curl and divergence; the pattern on the left
 565 is an unsteered unidirectional pattern, which intuitively should have zero di-
 566 vergence and curvature. While some of these patterns contain what can be
 567 considered curvature singularities at the sharp corners of the pattern, the
 568 zero curvature condition is still satisfied everywhere except at these points.
 569 While these regions may seem problematic for the turning radius manufac-
 570 turing constraint described in the previous sections, this problem can be

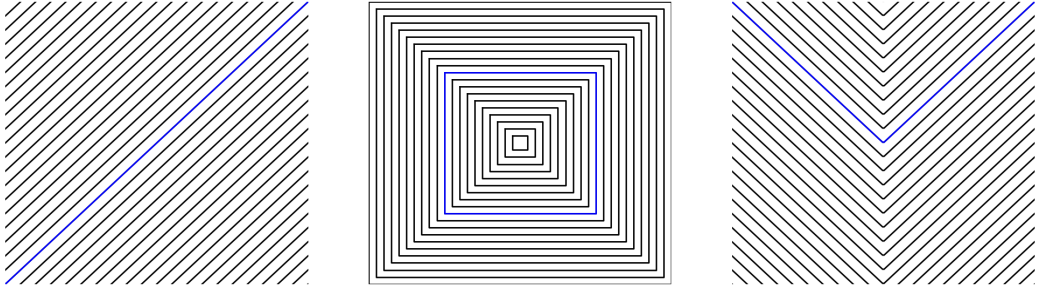


Figure 20: Example of Eikonal solutions with no divergence/curvature.

571 alleviated by having the AFP machine cut the tow at these corners, rotate
 572 the machine head, and continue laying in the new direction. If these re-
 573 gions occur frequently throughout the pattern, then the manufacturing of
 574 the pattern may become difficult.

575 These families of solutions represent the extreme limits on either the
 576 gaps/overlaps or fiber path curvature. The zero-divergence and zero-curl pat-
 577 terns have the desirable manufacturing properties of being free of gaps/overlaps
 578 and curvature, respectively. In general, tow patterns with superior structural
 579 performance can be achieved by allowing for some amount of both divergence
 580 and curvature throughout the pattern.

581 8. Conclusions

582 In this work, we show that tow paths of a general tow-steered pattern can
 583 be treated as the streamlines of a unit-vector field. Through this choice of
 584 definition, several manufacturing constraints can be intuitively related using
 585 vector calculus differential operators. In particular, we demonstrate that the
 586 curl of such a vector field is equivalent to the tow path curvature of the
 587 layup. Through further derivation, we also prove that the rate of growth

588 of gaps and overlaps is directly related to the divergence of the vector field.
589 Through these derived relationships, we find closed-form solutions for the
590 curvature, gap/overlap spacing, and gap/overlap sizes for two analytic tow
591 patterns.

592 These relationships then lead to the development of a conservative ap-
593 proximation of the minimum cut/add lengths for the AFP machine based
594 on the maximum and minimum divergence values for a given pattern. We
595 demonstrate the utility of this constraint in the context of a structural design
596 optimization problem. From the results of this optimization we show that the
597 resulting design features undesired tow path convergence regions when left
598 unconstrained. For a modest penalty in structural performance, we achieve
599 a realistic manufacturable design through the enforcement of the constraint.

600 Finally, through the use of a 2D scalar potential field and stream func-
601 tions, we derive the Eikonal PDE. The solution of this PDE yields a family
602 of gap/overlap-free and curvature-free tow patterns. The solution of the
603 Eikonal PDE motivates an alternate parametrization scheme for tow-steered
604 patterns that uses the fast marching scheme. The curvature and divergence
605 of the divergence-free and curvature-free patterns is related to the stream and
606 scalar potential function, respectively. This choice parametrization might be
607 desirable for designers that wish to the presence of gaps/overlaps or curvature
608 in the layup.

609 The formulation provided in this work may provide a better understand-
610 ing of the nature of gaps/overlaps and curvature for a general tow-steered
611 design. Through these relationships designers can identify regions of man-
612 ufacturing difficulty in the design without having numerically integrate or

613 layup the AFP tow paths. Furthermore, these relationships lead to simple
614 constraints for design optimization that provide bounds on the severity of
615 these regions in the layup.

616 **Acknowledgements**

617 This work was supported in part by the National Aeronautics and Space
618 Administration through award NNL15AA01C.

619 **References**

- 620 [1] A. Khani, S. IJsselmuiden, M. Abdalla, Z. Gurdal, Design of variable stiffness panels for maximum strength using lamination parameters, Composites Part B: Engineering 42 (2011) 546–552.
- 623 [2] C. Lopes, Z. Gurdal, P. Camanho, Tailoring for strength of composite steered-fibre panels with cutouts, Composites Part A: Applied Science and Manufacturing 41 (2010) 1760–1767.
- 626 [3] M. W. Hyer, R. F. Charette, Use of curvilinear fiber format in composite structure design, AIAA Journal 29 (1991) 1011–1015.
- 628 [4] S. T. Ijsselmuiden, M. M. Abdalla, Z. Gurdal, Optimization of variable-stiffness panels for maximum buckling load using lamination parameters, AIAA Journal 48 (2010) 134–143.
- 631 [5] S. Setoodeh, M. M. Abdalla, S. T. IJsselmuiden, Z. Gurdal, Design of variable-stiffness composite panels for maximum buckling load, Composite Structures 87 (2009) 109–117.

- 634 [6] M. Hyer, H. Lee, The use of curvilinear fiber format to improve buckling
635 resistance of composite plates with central circular holes, Composite
636 Structures 18 (1991) 239–261.
- 637 [7] J. M. van Campen, C. Kassapoglou, Z. Gurdal, Generating realistic lam-
638 inate fiber angle distributions for optimal variable stiffness laminates,
639 Composites Part B: Engineering 43 (2012) 354–360.
- 640 [8] Z. Wu, P. M. Weaver, G. Raju, B. C. Kim, Buckling analysis and opti-
641 misation of variable angle tow composite plates, Thin-Walled Structures
642 60 (2012) 163 – 172.
- 643 [9] T. J. Dodwell, R. Butler, A. T. Rhead, Optimum fiber steering of
644 composite plates for buckling and manufacturability, AIAA Journal 54
645 (2016) 1146–1149.
- 646 [10] D. M. Peeters, S. Hesse, M. M. Abdalla, Stacking sequence optimisation
647 of variable stiffness laminates with manufacturing constraints, Compos-
648 ite Structures 125 (2015) 596 – 604.
- 649 [11] P. Crothers, K. Drechsler, D. Feltin, I. Herszberg, T. Kruckenberg, Tai-
650 lored fibre placement to minimise stress concentrations, Composites
651 Part A: Applied Science and Manufacturing 28 (1997) 619–625.
- 652 [12] D. Jegley, B. Tatting, Z. Gurdal, Optimization of Elastically Tailored
653 Tow-Placed Plates with Holes, American Institute of Aeronautics and
654 Astronautics.
- 655 [13] G. G. Lozano, A. Tiwari, C. Turner, S. Astwood, A review on design for
656 manufacture of variable stiffness composite laminates, Proceedings of

- 657 the Institution of Mechanical Engineers, Part B: Journal of Engineering
658 Manufacture 230 (2015) 981–992.
- 659 [14] B. F. Tatting, Z. Gurdal, Design and manufacture of elastically tailored
660 tow placed plates, 2002.
- 661 [15] L. Parnas, S. Oral, . Ceyhan, Optimum design of composite structures
662 with curved fiber courses, Composites Science and Technology 63 (2003)
663 1071–1082.
- 664 [16] A. W. Blom, M. M. Abdalla, Z. Gurdal, Optimization of course locations
665 in fiber-placed panels for general fiber angle distributions, Composites
666 Science and Technology 70 (2010) 564–570.
- 667 [17] Z. Gurdal, B. Tatting, K. Wu, Variable stiffness composite panels: Ef-
668 fects of stiffness variation on the in-plane and buckling response, Com-
669 posites Part A: Applied Science and Manufacturing 39 (2008) 911–922.
- 670 [18] R. Olmedo, Z. Gurdal, Buckling response of laminates with spatially
671 varying fiber orientations, Structures, Structural Dynamics, and Ma-
672 terials and Co-located Conferences, American Institute of Aeronautics
673 and Astronautics, 1993.
- 674 [19] B. Tatting, Z. Gurdal, Design and manufacture of elastically tailored
675 tow placed plates, Technical Report NASA/CR-2002-211919, NASA,
676 Langley Research Center, Hampton, VA, 2002.
- 677 [20] A. W. Blom, Structural Performance of Fiber-Placed, Variable-Stiffness
678 Composite Conical and Cylindrical Shells, Ph.D. thesis, Delft University
679 of Technology, 2011.

- 680 [21] G. J. Kennedy, J. R. R. A. Martins, A parallel finite-element framework
681 for large-scale gradient-based design optimization of high-performance
682 structures, *Finite Elements in Analysis and Design* 87 (2014) 56–73.
- 683 [22] J. R. R. A. Martins, J. T. Hwang, Review and unification of methods for
684 computing derivatives of multidisciplinary computational models, *AIAA Journal* 51 (2013) 2582–2599.
- 686 [23] P. E. Gill, W. Murray, M. A. Saunders, An SQP algorithm for large-scale
687 constrained optimization, *Society for Industrial and Applied Mathematics* 47 (2005).
- 689 [24] G. Kreisselmeier, R. Steinhauser, Systematic control design by optimiz-
690 ing a vector performance index, in: International Federation of Ac-
691 tive Controls Syposium on Computer-Aided Design of Control Systems,
692 Zurich, Switzerland.
- 693 [25] A. B. Lambe, J. R. R. A. Martins, G. J. Kennedy, An evaluation of con-
694 straint aggregation strategies for wing box mass minimization, *Struc-
695 tural and Multidisciplinary Optimization* (2016). (In press).
- 696 [26] T. R. Brooks, G. J. Kennedy, J. R. R. A. Martins, High-fidelity
697 aerostructural optimization of a high aspect ratio tow-steered wing,
698 in: 57th AIAA/ASCE/AHS/ASC Structures, Structural Dynamics, and
699 Materials Conference, American Institute of Aeronautics and Astronau-
700 tics, 2016.
- 701 [27] O. Stodieck, J. E. Cooper, P. M. Weaver, P. Kealy, Aeroelastic tailor-

- 702 ing of a representative wing box using tow-steered composites, AIAA
703 Journal 55 (2017) 1425–1439.
- 704 [28] J. A. Sethian, A fast marching level set method for monotonically ad-
705 vancing fronts, Proceedings of the National Academy of Sciences 93
706 (1996) 1591–1595.
- 707 [29] M. Bruyneel, S. Zein, A modified fast marching method for defining
708 fiber placement trajectories over meshes, Computers & Structures 125
709 (2013) 45–52.
- 710 [30] C. J. Brampton, K. C. Wu, H. A. Kim, New optimization method for
711 steered fiber composites using the level set method, Struct. Multidiscip.
712 Optim. 52 (2015) 493–505.
- 713 [31] E. Lemaire, S. Zein, M. Bruyneel, Optimization of composite structures
714 with curved fiber trajectories, Composite Structures 131 (2015) 895 –
715 904.